DOI: 10.1002/ejic.201000586

Self-Organization by Chiral Recognition Based on *ad hoc* Chiral Pockets in Cyclotriphosphazenes with Binaphthoxy and Biphenoxy Substituents: An X-ray, NMR and Computational Study

José L. García Álvarez,[a] Maria E. Amato,[b] Giuseppe M. Lombardo,[b] Gabino A. Carriedo,*[a] and Francesco Punzo*[b]

Keywords: Spiro compounds / Phosphazenes / Chiral recognition / X-ray diffraction / NMR spectroscopy / Molecular mechanics

The chiral cyclic triphosphazenes (*R*)-(–)-[$N_3P_3(O_2C_{20}H_{12})$-$(O_2C_{12}H_8)Cl_2$] (**I**) and (*R*,*R*)-(–) [$N_3P_3(O_2C_{20}H_{12})_2(O_2C_{12}H_8)$] (**II**), prepared by sequential substitution of [$N_3P_3Cl_6$] using (*R*)-2,2′-dihydroxy-1,1′-binaphthyl, 2,2′-dihydroxy-1,1′-biphenyl and Cs_2CO_3 in acetone, have been investigated by single-crystal X-ray diffraction, variable-temperature NMR spectroscopy in solution and MM calculations under periodic boundary conditions in the gas state. In both compounds only the diastereomer corresponding to the (*R*)-biphenoxy configuration is present in the solid state. In spite of the existence of quite large voids potentially occupied by solvents, the configuration adopted by the biphenoxy substituents is solely determined by packing interactions consisting of definite preferential supramolecular interactions between a biphenoxy group of one molecule and the chiral pocket created between the biphenoxy and binaphthoxy groups of another molecule. A network of T-shaped non-covalent interactions ensures an efficient chiral discrimination. The *in silico* simulations confirmed this hypothesis. Both the concentration-dependence and temperature-variable ^{1}H NMR spectra in solution confirmed this behaviour showing that on lowering the temperature one of the two diasteroisomers vanished after conversion into the more stable atropisomer as a consequence of chiral induction of the (*R*)-binaphthyl system on the (*R*)-biphenyl configuration. In further agreement with the X-ray structure as well as with the energy distribution resulting from the *in silico* calculations, the ^{1}H NMR spectra show the dependence of the chemical shift on concentration, which suggests the presence of aggregates in solution. Therefore molecules **I** and **II** are capable of a special type of self-organization by chiral recognition based on the *ad hoc* generation of chiral pockets.

Introduction

Phosphazenes are compounds based on skeletal consecutive –N=PR_2– bonds forming either cyclic molecules or linear high M_w polymers. The latter are very important materials with interest in fundamental and applied chemistry.[1] Cyclic phosphazenes $[NPR_2]_n$ (n = 3–8) have always been considered as useful models to approach the structure and chemistry of high M_w polymers[2] and the bonding of the –NPR_2– rings has been repeatedly revisited.[3] A recent topological analysis of the chemical bond in molecules of $[P_nN_nX_{2n}]$ (X = H, F, Cl; n = 2, 3, 4) has shown that the formation of non-covalent intermolecular P···N interactions along the symmetry axis helps the participation of cyclophosphazenes in self-assembling supramolecular aggregates.[4] Since the early review[5] of Allcock in 1972, numerous cyclophosphazenes with a great variety of structures and substituents have been synthesized, frequently with the purpose of designing special multi-dentate ligands to form complexes with transition metals.[6]

A special type of cyclophosphazenes are the spirocyclic phosphazenes,[7] that is, compounds in which the endocyclic phosphazene phosphorus atoms are part of another ring, frequently consisting of dioxyaryl or dioxybiaryl moieties. Recently, various cyclotetraphosphazenes with 2,2′-dioxybiphenyl substituents have been characterized by X-ray diffraction to show the importance of π–π and π–H interactions in their crystals.[8] Spirocyclic phosphazenes are of particular interest because of their ability to act as host molecules,[9] as well as to induce inclusion polymerization.[10] Recent calculations on tris(*o*-phenylenedioxy)cyclotriphosphazene and related cycles have shown that the electron-donating capacity of the entire molecule is very dependent on that of the side-group[11] and that good electron-donating capacity and the paddle wheel molecular shape make them good candidates for organic superconductors.[12]

In previous work we described the X-ray crystal structure of the spiro(2,2′-dioxybiphenyl)tetrachlorocyclo-

[a] Departamento de Química Orgánica e Inorgánica, Facultad de Química, Universidad de Oviedo,
33071 Oviedo Spain
E-mail: gac@uniovi.es
[b] Dipartimento di Scienze Chimiche, Università di Catania,
Viale Andrea Doria, 6, 95125 Catania, Italy
Fax: +39-095-580138
E-mail: fpunzo@unict.it

Supporting information for this article is available on the WWW under http://dx.doi.org/10.1002/ejic.201000586.

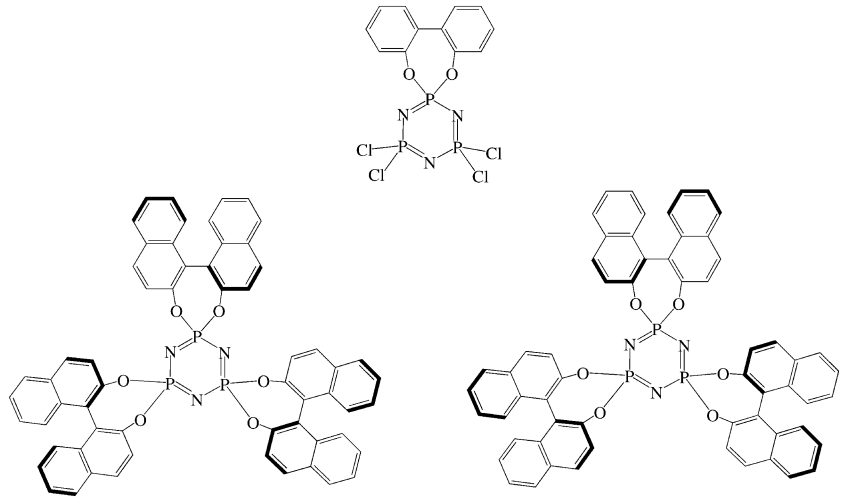

Scheme 1. Compound $[N_3P_3Cl_4(O_2C_{12}H_8)]$ and the configuration of (*R*,*R*,*R*)-(–)-$[N_3P_3(O_2C_{20}H_{12})_3]$ (left) and (*S*,*S*,*S*)-(+)-$[N_3P_3(O_2C_{20}H_{12})_3]$ (right).

triphosphazene $[N_3P_3Cl_4(O_2C_{12}H_8)]$ (Scheme 1). It was shown that, as found in the corresponding bis- $N_3P_3Cl_2(O_2C_{12}H_8)_2]$ and tris $[N_3P_3(O_2C_{12}H_8)_3]$ derivatives, the packing is controlled by weak π interactions. These are particularly effective between two molecules with the same absolute configuration, that is, *R* or *S*, whereas they are negligible between those with opposite configurations, producing a chiral discrimination in the solid state.[13] The 2,2′-dioxybiphenylphosphazene unit $[NP(O_2C_{12}H_8)]$ may adopt either the *R* or *S* configurations, giving rise to stereoisomers that rapidly interconvert in solution.[14] In contrast, the interconversion energy barrier is much larger for the 2,2′-dioxybinaphthyl analogues. As a consequence, the optically active pure atropisomers of the tris derivative, (*R*,*R*,*R*)-(–)-$[N_3P_3(O_2C_{20}H_{12})_3]$ and (*S*,*S*,*S*)-(+)-$[N_3P_3(O_2C_{20}H_{12})_3]$, could be isolated[15] (Scheme 1).

In the solid state, because of the weak packing interactions caused by steric hindrance, the crystals of these compounds tend to be very easily fragmented, forming amorphous or semi-crystalline batches with crystals that are too small to be accurately analysed by X-ray diffraction. However, a combination of theoretical (molecular dynamics) and experimental (X-ray diffraction and NMR) techniques provided a viable tool for determining the molecular and crystal structures of various systems, which would otherwise be inaccessible by a single technique.[13,14,16,17] In particular, the structure and molecular assembly of the solid (*S*,*S*,*S*)-(+)-$[N_3P_3(O_2C_{20}H_{12})_3]$ could be resolved by a combination of molecular dynamics (MD) and large-angle X-ray scattering (LAXS) measurements in the energy-dispersive X-ray diffraction (EDXD) mode of scanning.[17] Whereas in another work,[16h] structural data and molecular assembly of the amorphous isotactic polymeric counterpart (*R*)-poly(2,2′-dioxy-1,1′-binaphthyl)phosphazene were attained through accurate MD refinement of the radial distribution function (RDF) curve performed by standard MD

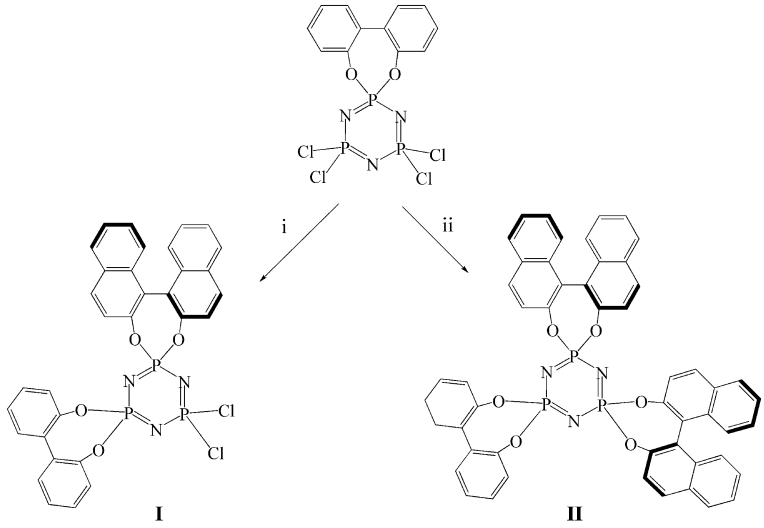

Scheme 2. Reagents and conditions: i) and ii) (*R*)-binaphthol (1:1 at room temp. or 1:2 at reflux) and Cs_2CO_3 in acetone.

simulations implemented with an added biasing potential to reproduce the experimental curve of the static structure function (SF) $i(q)$.

On the basis that the interactions between binaphthoxy groups with fixed absolute configurations and the atropisomerizable biphenoxy groups could lead to stereochemical discrimination in solution or in the solid state, we considered the synthesis of novel cyclic phoshazenes with both types of dioxybiaryls in the same molecule of interest. In this paper we report that the new chiral triphosphazenes (*R*)-(–)-$[N_3P_3(O_2C_{20}H_{12})(O_2C_{12}H_8)Cl_2]$ (**I**) and (*R*,*R*)-(–)-$[N_3P_3(O_2C_{20}H_{12})_2(O_2C_{12}H_8)]$ (**II**; Scheme 2), easily prepared from $[N_3P_3Cl_6]$ via $[N_3P_3(O_2C_{12}H_8)Cl_4]$ by using the Cs_2CO_3/acetone method,[18] form an interesting self-organizing system in which chiral recognition is guided by the creation of chiral pockets originating between a biphenoxy group on one molecule and the biphenoxy and binaphthoxy groups of another molecule. This is supported by X-ray crystal structure determination, variable-temperature and -concentration ^{1}H NMR analyses in solution and MM calculations with the formerly developed and validated force field (FF).[16d,16e] Therefore the self-assembly of **I** and **II** is an example of supramolecular synthesis[19] based on chiral recognition.

Results and Discussion

Compound **I** crystallized in a very inefficient way as a consequence of its efforts to minimize the interactions between the chlorine atoms present in the molecule (Figure 1). No packing index[20] was calculated as a result of the disorder present in the structure. A CH_2Cl_2 molecule is present in the crystal structure; its detection is justified by the fact that it is one of the solvents used during the synthesis of the compound. Two major symmetrical voids can host other disordered solvent molecules. The total potential solvent volume is 524.7 Å^3, which represents 14.9% of the total cell volume. Both voids have a volume of 262 Å^3. This is compatible with the presence of four other non-resolved and disordered CH_2Cl_2 molecules. The possible and alternative presence of (eight) molecules of acetone, also used during the synthesis, can be discarded as the IR spectrum showed no signals at 1720 cm^{-1} corresponding to the CO group. No further attempts were made to calculate and model the unassigned electron density, not condensed into enough isolated and sharp peaks as the already modelled CH_2Cl_2 molecule present in the structure is already disordered. Further details are presented in the Supporting Information.

Unlike **I**, compound **II** has a good packing index[20] (62.1%; Figure 2). No solvent molecules were detected in the crystal structure although there are potential solvent accessible voids. The total potential solvent area is 557.4 Å^3, which represents 12.5% of the total cell volume. Two major areas, both with a volume of 132 Å^3, were identified. This volume could be compatible with the presence of two non-resolved and disordered CH_2Cl_2 molecules. Once again the presence of acetone was ruled out by the IR spectrum. As for compound **I**, the potential presence of disordered solvent was neither further investigated nor modelled. Further details are presented in the Supporting Information.

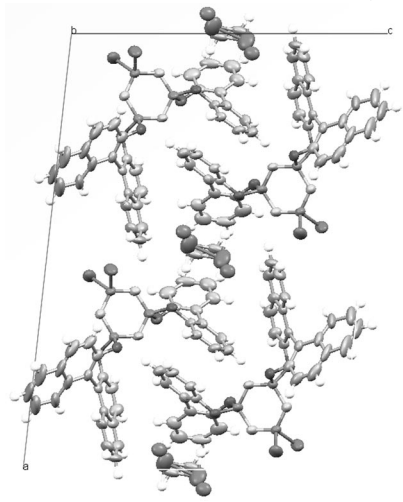

Figure 1. Crystal packing of **I** viewed along the *b* axis. Hydrogen atoms are shown as fixed-size spheres of an arbitrary radius of 0.30 Å and the ellipsoid probability level set to 50% for clarity. A disordered dichloromethane molecule is present with a halved atom occupancy factor.

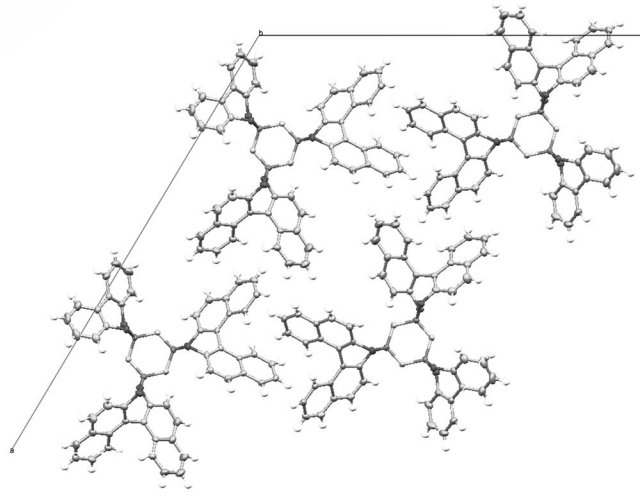

Figure 2. Crystal packing of **II** viewed along the *b* axis. Hydrogen atoms are shown as fixed-size spheres of an arbitrary radius of 0.30 Å and the ellipsoid probability level set to 50% for clarity.

As the seven-membered ring conformation, that is, the rings resulting from the connection of the phosphazenic ring with the binaphthoxy or biphenoxy rings, is crucial for the configuration of the naphthoxy or phenoxy moieties a ring-puckering analysis, that is, Cremer and Pople (C&P) analysis,[21a] was performed on both compounds to ensure that the absolute configuration, the pivot atom and the cyclic sense agree in order to be able to perform a comparison of the puckering for different rings.[21b] The ring-puckering can be represented by a single amplitude-phase pair (q_2 and ϕ_2) and a single puckering coordinate q_3 in the case of six-

Table 1. Ring-puckering coordinates for the Cremer and Pople analysis performed on the seven-membered rings in both **I** and **II** and the resulting conformation.

	Seven-membered ring	Q [Å]	q_2 [Å]	ϕ_2 [°]	q_3 [Å]	ϕ_3 [°]	Conformation
I	P(2)–O(8)–C(11)–C(17)–C(26)–C(15)–O(9)	1.001(5)	0.998(5)	89.9(3)	0.083(6)	88(3)	twisted boat
I	P(3)–O(7)–C(21)–C(25)–C(32)–C(28)–O(10)	0.906(5)	0.898(5)	85.1(3)	0.125(6)	73(2)	–
II	P(1)–O(43)–C(44)–C(45)–C(46)–C(47)–O(48)	0.963(3)	0.961(3)	89.88(18)	0.072(3)	93(2)	twisted boat
II	P(3)–O(21)–C(22)–C(23)–C(24)–C(25)–O(26)	1.001(3)	0.996(3)	93.87(18)	0.097(3)	125.4(18)	–
II	P(5)–O(7)–C(8)–C(9)–C(10)–C(11)–O(12)	0.916(3)	0.910(3)	268.4(2)	0.107(4)	275.7(15)	–

membered rings in which there are three puckering degrees of freedom or by adding another parameter (ϕ_3) for seven-membered rings in which there is an additional degree of freedom, that is, there are a couple of amplitude-phase pairs. This enables the immediate quantification and comparison of the different examined rings. The same results can be obtained by using spherical coordinates Q, θ and ϕ, as also shown in the Supporting Information for six-membered rings. Therefore the total puckering amplitude can be defined by Equation (1).[21a] As reported in Table 1, the most common conformation[21c] is a twisted boat (TB).

$$\sum_i n_i^2 = q_2^2 + q_3^2 = Q^2 \quad (1)$$

In the analysis of **I** the solvent molecules were omitted to allow the software to analyse rings with the number of atoms greater than 6.[21d,21e] Once more, C&P analysis revealed close similarities between **I** and **II**. All the other details of the C&P analysis are described in the Supporting Information.

Although in **I** and **II** there is no evidence of hydrogen bonding nor of possible π-stacking interactions between aromatic rings, a complex network of T-shaped non-covalent aromatic interactions (T interaction) could be detected (see Figures 3 and 4).

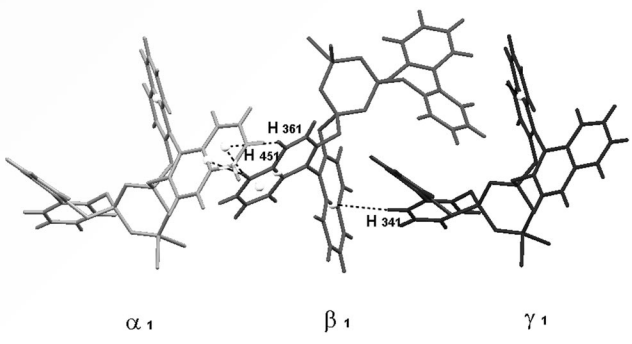

Figure 3. Molecular assembly of **I**. The chiral recognition between molecules due to a T-shaped interaction is denoted by a dotted line.

A detailed description of the resulting network is provided in the Supporting Information. Recently,[22a–22e] theoretical calculations revealed the T interactions in small aromatic rings to have a binding energy very similar to those of π-stacking non-covalent interactions.

The above-mentioned interactions are clearly possible in both **I** and **II** between conformers having the found configuration (all *R* or all *S*) only. There is therefore evidence of a chiral interaction between different fragments in the solid state.

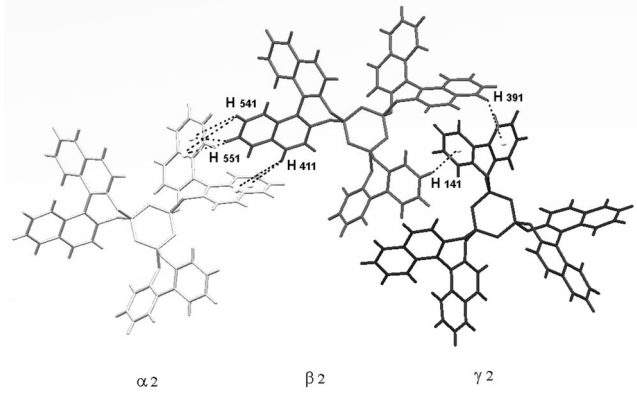

Figure 4. Molecular assembly of **I**. The chiral recognition between molecules due to a T-shaped interaction is denoted by a dotted line.

MM calculations were performed on **I** by analysing the system as a single molecule, as dimers as well as under periodic boundary conditions (PBC). Although the calculation of the single molecule is generally considered a starting point, we first performed calculations under PBC to confirm the good quality of the force field (FF), which has already proven to be in good agreement with the experimental results for similar phosphazenic compounds,[14,16d,16e,17] and its ability to reproduce the picture already described by X-ray diffraction analysis. This was achieved by fixing the cell parameters using the experimental conformation **A**, that is, *R*,*R* (**A1**) or *S*,*S* (**A2**), and comparing the results with the a hypothetical inverse conformation **B**, that is, *R*,*S* (**B1**) or *S*,*R* (**B2**). As shown in Table 2, a comparison between the total energy values of conformations **A** and **B** shows, as expected, that **A** is more stable than **B**, which confirms the ability of the FF to describe a picture close to the experimental one.

The results of the calculations performed allowing the unit cell to fully relax (Table 3), to allow **B** to fit comfortably into it, show that even in this case **A** is more stable than **B**.

The cell parameters resulting from this calculation match very well those determined by X-ray diffraction analysis for **A**, whereas for **B** they are slightly different in terms of both cell lengths and angles, as shown in Table 4.

Having checked the reliability of the FF we compared **A1** and **B1**. The stand-alone energies of the two different

Table 2. Energy of **I** with fixed cell parameters in the crystal phase in the *R*,*R* (**A1**), *S*,*S* (**A2**), *R*,*S* (**B1**) or *S*,*R* (**B2**) conformation.

	Energy [kcal mol^{-1}]	
	A1 or **A2**	**B1** or **B2**
Total energy	– 470.552	–436.235
Bonds	20.506	20.237
Angles	70.597	75.008
Torsions	251.132	259.088
Inversions	0.534	0.791
Urey–Bradley	23.689	23.670
van der Waals	–54.012	–39.218
Electrostatic	–782.997	–775.812

Table 3. Energy of fully relaxed **I** in the crystal phase in the *R*,*R* (**A1**), *S*,*S* (**A2**), *R*,*S* (**B1**) or *S*,*R* (**B2**) conformation.

	Energy [kcal mol^{-1}]	
	A1 or **A2**	**B1** or **B2**
Total energy	–471.987	–448.857
Bonds	20.189	20.351
Angles	70.578	72.427
Torsions	251.426	257.273
Inversions	0.516	0.621
Urey–Bradley	23.181	25.824
van der Waals	–55.498	–50.501
Electrostatic	–782.379	–774.850

Table 4. Crystal cell parameters of fully relaxed **I** in the *R*,*R* (**A1**), *S*,*S* (**A2**), *R*,*S* (**B1**) or *S*,*R* (**B2**) conformation compared with the experimental (single-crystal X-ray diffraction) values.

	X-ray	**A1** or **A2**	**B1** or **B2**
a [Å]	26. 0158(9)	26.117943	24.698344
b [Å]	7.2275(2)	7.112827	7.740241
c [Å]	18.8203(5)	19.081911	18.44131
α [°]	90	90.4292	88.65884
β [°]	96.336(3)	97.27712	95.69473
γ [°]	90	89.58529	92.42162

conformers are very similar, as shown in Table 5, which suggests that any considerable difference resulting from the interaction between the units should not be ascribed to the difference in energy between the molecules themselves.

The analysis of the dimers of **A** or **B** once again indicated a systematically lower energy for **A** compared with **B**. Most of this balance is due to the weaker van der Waals interactions present in **B**, as evident from Table 5. The lower overall energy (per monomer) of the dimeric system as compared with the monomeric one confirms that the former is more stable so explaining the tendency of the system to pack in couples of dimers, as inferred by the X-ray solid-state analysis.

Passing to **II**, the calculations were performed considering only, as for **I**, the two possible configurations of the biphenyl moieties, namely *S* (**C**; real and experimental one) and *R* (**D**). There was no need to confirm once again the validity of the FF and therefore the calculations were performed by considering only the fully relaxed crystallographic cell. Although both **C** and **D** have cell parameters very similar to the corresponding values in the real cell, as confirmed by X-ray diffraction analysis, a closer look at Table 6 shows that **C** differs less from the experimental values confirming that the FF describes quite well the experimental situation.

Table 6. Crystal cell parameters of fully relaxed **II** with the biphenyl group in the *S* (**C**) or *R* (**D**) conformation as compared with the experimental (single-crystal X-ray diffraction) values.

	X-ray	**C**	**D**
a [Å]	32. 9552(5)	33.1045	33.1515
b [Å]	5.59770(10)	5.75940	5.81396
c [Å]	28.2450(7)	28.3125	28.5919
α [°]	90	90.0144	89.9474
β [°]	120.9078(8)	120.898	119.677
γ [°]	90	89.9936	90.1123

A comparison of the energies of **C** and **D** reported in Table 7 highlights the fact that **C** is systematically more stable than **D**.

Table 7. Energy per molecule of fully relaxed **II** in the crystal phase with the *S* (**C**) or *R* (**D**) conformation at the biphenyl group.

	Energy [kcal mol^{-1}]	
	C	**D**
Total energy	–59.086	– 55.783
Bonds	6.146	5.934
Angles	17.111	16.799
Torsions	109.398	110.121
Inversions	0.231	0.248
Urey–Bradley	7.546	7.483
van der Waals	–3.187	0.429
Electrostatic	–196.331	–196.795

Table 5. Gas-phase energy of the fully relaxed monomers and dimers of A and B and the relative energy differences between monomers and dimers.

	Energy [kcal mol^{-1}]					
	Monomer **A**	Monomer **B**	ΔE[a] monomer	Dimer **A**	Dimer **B**	ΔE[a] dimer
Total energy	–71.695	–71.414	0.281	–79.444	–77.835	1.609
Bonds	5.043	4.953	–0.090	5.191	5.383	0.192
Angles	17.335	17.121	–0.214	17.923	18.408	0.485
Torsions	63.185	64.003	0.818	62.369	61.600	–0.769
Inversions	0.100	0.099	–0.001	0.131	0.129	–0.002
Urey–Bradley	5.909	5.500	–0.409	6.545	6.411	–0.134
van der Waals	30.114	30.075	–0.039	21.813	23.680	1.866
Electrostatic	–193.382	–193.165	0.217	–193.416	–193.446	–0.03

[a] $\Delta E = E_B - E_A$.

Table 8. Energy per molecule with the *S* (**C**) or *R* (**D**) conformation at the biphenyl group for monomers and dimers obtained by approaching each others with the binaphthyls **3** or the biphenyls **4**.

	Energy [kcal mol^{-1}]								
	Monomer **C**	Monomer **D**	ΔE[a] Monomer	Dimer **C3**	Dimer **D3**	ΔE[a] Dimer	Dimer **C4**	Dimer **D4**	ΔE[a] Dimer
Total energy	–5.661	–5.905	–0.244	–7.655	–8.112	–0.457	–11.588	–10.087	1.501
Bonds	6.653	6.533	–0.120	6.574	6.548	–0.026	6.507	6.615	0.108
Angles	17.474	17.123	–0.351	17.418	17.265	–0153	17.278	17.474	0.196
Torsions	107.644	108.224	0.580	107.719	108.180	0.461	108.406	107.889	–0.517
Inversions	0.153	0.138	–0.015	0.156	0.141	–0.015	0.150	0.136	–0.014
Urey–Bradley	6.535	6.378	–0.157	6.596	6.356	–0.240	6.138	6.525	0.387
Van der Waals	52.072	52.521	0.449	50.203	50.375	0.172	46.627	48.204	1.577
Electrostatic	–196.192	–196.822	–0.630	–196.321	–196.977	–0.656	–196.694	–196.930	–0.236

[a] $\Delta E = E_D - E_C$.

Once again the greatest difference in energy can be attributed to the van der Waals interactions, which are slightly more favourable in **C** than in **D**. An analysis of the standalone molecules of **C** and **D** shows that both conformers have almost the same energy. Passing to the dimers, we decided to study two possible interactions in this system: the first in which the two molecules are docked to grab each other by the pockets formed between two binaphthyls **3** and the second in which the two molecules dock to form pockets through interactions with the binaphthyls and biphenyls **4**. Both types of interactions are actually experienced in the crystal unit cell. The first are clearly evident inside the cell, whereas the second are present in the crystal between the adjacent unit cells. Once again we need to compare **C** and **D** taking into account in this case the two different ways the dimers can interact between themselves, that is, **3** or **4**. As shown in Table 8, there are some important results that can be highlighted: first of all, comparing the energy values, it is evident that the dimers are systematically more stable than the monomers, no matter what the configuration.

Furthermore, for the first time **C** is not as stable as **D** as in the former cases when considering interaction type 3, but it turns out once again to be more stable when considering interactions of type 4. The interactions between dimers are clearly more efficient in 4 than in 3, which suggests a preferential interaction by biphenyls; these biphenyls must be in the C conformation, the experimental one, to interact properly.

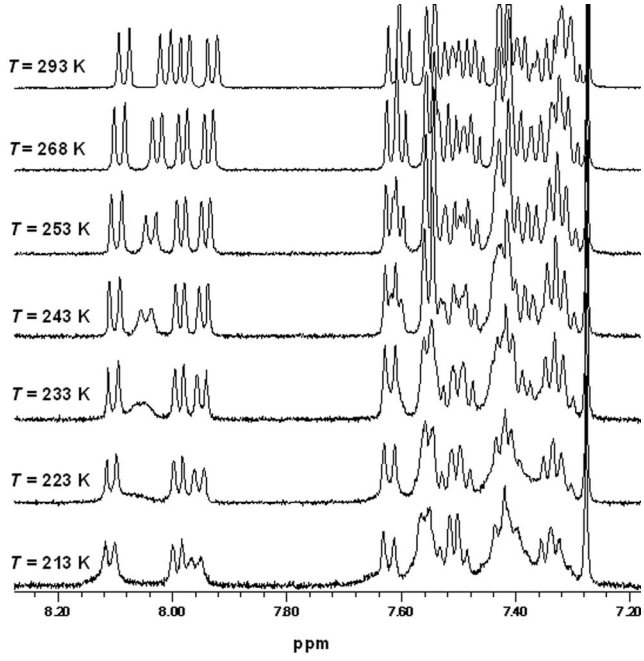

Figure 5. Temperature-dependent ^{1}H NMR spectra (500 MHz) of **I** in $CDCl_3$.

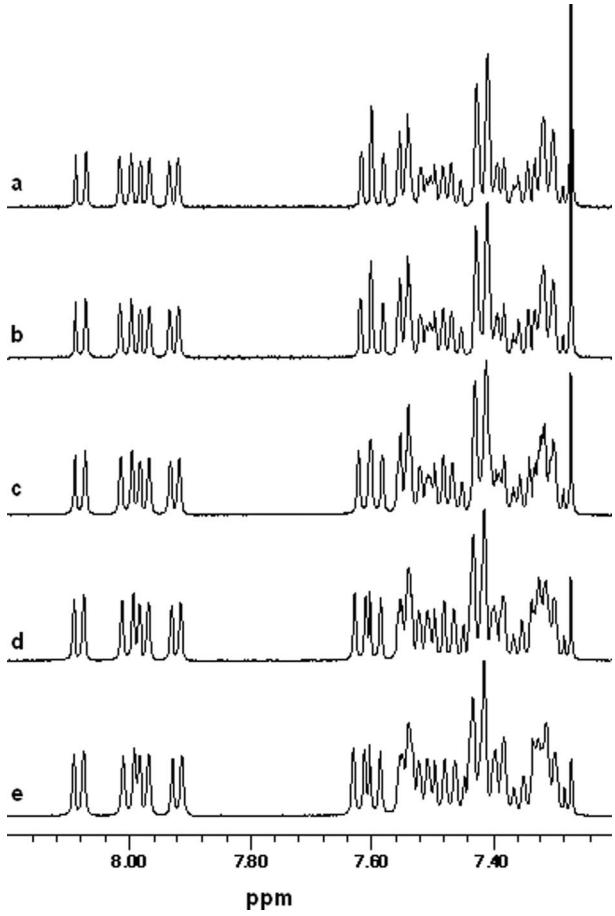

Figure 6. ^{1}H NMR spectra (500 MHz, 300 K, $CDCl_3$) of **I** as a function of concentration. (a) 4.4×10^{-6} M; (b) 1.5×10^{-5} M; (c) 2.7×10^{-5} M; (d) 5×10^{-5} M; (e) 6.3×10^{-5} M.

As shown in the Supporting Information, the ^{1}H NMR spectra of **I** and **II** in solution reveal a pattern of severely overlapping sets of signals in the aromatic region originated by both 2,2′-dioxybinaphthyl and 2,2′-dioxybiphenyl groups. Although the superposition of the signals makes a careful observation of the biphenyloxy moiety difficult, the binaphthyloxy system was easily observed as some signals are well resolved. Binaphthyl protons give rise to a double set of signals in both compounds, which indicates that, at room temperature, two diastereoisomers are present as a consequence of the atropisomerization of the biphenylic system. The well-separated downfield signals of the binaphthyloxy groups allow the assumption that *R* and *S* configurations of the stereolabile biphenyl group are equally populated. Moreover, the variable-temperature ^{1}H NMR analysis (300–213 K, $CDCl_3$) reported in Figure 5 shows that, on cooling, the spectrum of **I** becomes simpler both for the binaphthyl and biphenyl sets of signals.

This can be interpreted to be a result of the disappearance of one of the two diastereoisomers, which is converted into the most stable atropisomer at low temperature. This feature is in agreement with the chiral induction of the *R* binaphthyl system on the *R* biphenyl configuration as already observed in the solid state by X-ray analysis as well as with the energy distribution resulting from the *in silico* calculations. The same analysis was not performed on **II** as the low solubility of this compound, magnified on lowering the temperature, prevents the recording of the spectra. The resulting analysis would not allow the appreciation of any possible effect.

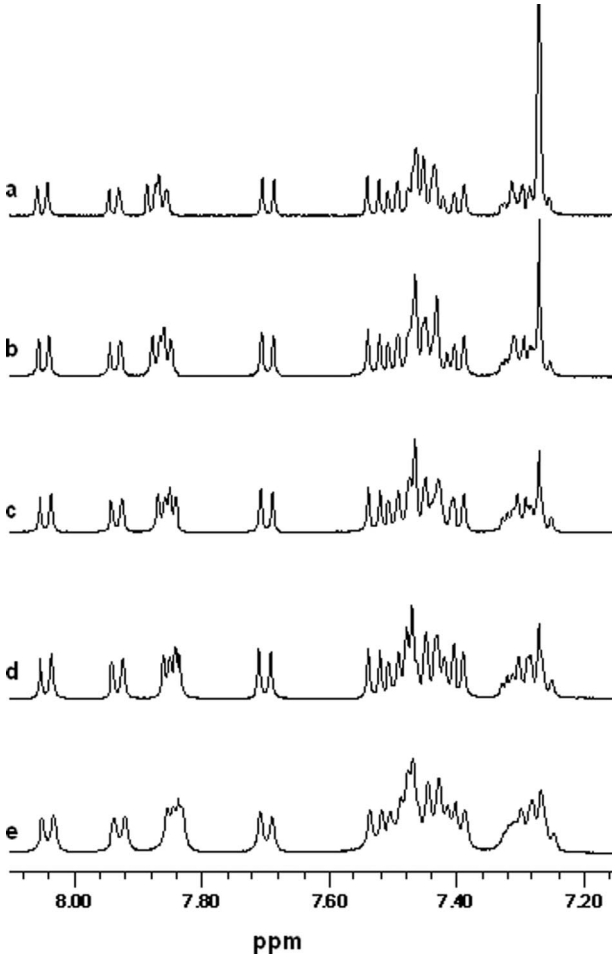

Figure 7. ^{1}H NMR spectra (500 MHz, 300 K, $CDCl_3$) of **II** as a function of concentration. (a) 4.4×10^{-6} M; (b) 1.5×10^{-5} M; (c) 2.7×10^{-5} M; (d) 5×10^{-5} M; (e) 6.3×10^{-5} M.

The ability demonstrated by **I** and **II** to form dimers in the solid state, also confirmed by theoretical calculation, is present even in solution. The analysis of the ^{1}H NMR spectra of **I** and **II** (room temperature, $CDCl_3$) presented in Figures 6 and 7 shows the dependence of the chemical shift on the concentration, which indicates that aggregates are present in solution, although without any diastereoisomeric predominance.

Conclusions

The X-ray structures of the chiral cyclic triphosphazenes (*R*)-(–)-[$N_3P_3(O_2C_{20}H_{12})(O_2C_{12}H_8)Cl_2$] (**I**) and (*R*,*R*)-(–)-[$N_3P_3(O_2C_{20}H_{12})_2(O_2C_{12}H_8)$] (**II**) contain only the diastereomer corresponding to the (*R*)-biphenoxy configuration. The packing interactions are guided by definite preferential supramolecular interactions between a biphenoxy group of one molecule and a chiral pocket created between the biphenoxy and binaphthoxy groups of another molecule. A network of T-shaped non-covalent interactions makes the chiral discrimination more efficient. The *in silico* simulations confirmed that the packing in the crystal is achieved by the relative movements of the molecules, which, seeking better matching, induce the formation of a chiral pocket leading to chiral discrimination. The variable-temperature ^{1}H NMR spectra in solution at various concentrations further supports this behaviour showing the gradual fading of diastereoisomers that convert into the more stable atropisomers as a consequence of the chiral induction of the (*R*)-binaphthyl system on the (*R*)-biphenyl configuration. Therefore, molecules **I** and **II** are capable of a special type of self-organization by chiral recognition based on the *ad hoc* generation of chiral pockets.

Experimental Section

General: Information on the instrumentation, figures showing in detail the molecular packing as well as NMR spectra are reported in the Supporting Information. All reactions were carried out under dry N_2. Cs_2CO_3 was dried at 140 °C prior to use. The acetone was distilled twice from Na_2SO_4. The THF was treated with KOH and distilled twice from Na in the presence of benzophenone. [$N_3P_3Cl_6$] (Strem), (*R*)-2,2′-dihydroxy-1,1′-binaphthyl [(+)-binaphthol] with $[\alpha]_D^{25}$ = +33° (*c* = 1, THF) (Merck) and 2,2′-dihydroxy-1,1′-biphenyl (Aldrich) were used as purchased.

(*R*)-(–)-[($N_3P_3O_2C_{20}H_{12}$)($O_2C_{12}H_8$)Cl_2] (I): [$N_3P_3(O_2C_{12}H_8)Cl_4$] (0.685 g, 1.49 mmol), (+)-binaphthol (0.417 g, 1.46 mmol), Cs_2CO_3 (1.453 g, 4.46 mmol) and acetone (22 mL) were stirred at room temperature for 1 h under an inert atmosphere. Acetone was then evaporated in a rotavapor under high vacuum. The remaining solid was extracted with CH_2Cl_2 (2 × 50 mL) and filtered through Celite/

activated carbon. The solution was concentrated and the product was crystallized from CH_2Cl_2/hexane to give large needles; yield 0.538 g (53.7%). $[\alpha]_D^{25}$ = –172.9°mL dm^{-1} g^{-1} (c = 10 mg mL^{-1}, $CHCl_3$). IR (KBr): $\tilde{\nu}$ = 3068.9 (w), 1590.5 (w), 1475.9 (w), 1465.3 (w), 1437.8 (w), 1277.5 (w), 1251.8 (m), 1228.6 (m), 1202.6 (s), 1181.4 (vs), 1095.6 (m), 1070.6 (w), 1001.7 (w), 970.4 (s), 949.5 (w), 922.3 (w), 904.2 (w), 887.0 (w), 854.5 (w), 844.9 (w), 813.8 (w), 783.7 (w), 754.5 (w), 736.4 (w), 717.5 (w), 695.9 (w), 656.3 (w) cm^{-1}. $^{31}P\{^1H\}$ NMR ($CDCl_3$): δ = 29.8 (t, J = 78.55 Hz), 21.5 (dd, J = 87.58, 79.45 Hz), 20.0 (dd, J = 87.58, 76.75 Hz) ppm.

$[N_3P_3(O_2C_{12}H_8)\{(+)\text{-}O_2C_{20}H_{12}\}_2]$ (II): $[N_3P_3(O_2C_{12}H_8)Cl_4]$ (0.500 g, 1.08 mmol), (+)-binaphthol (0.653 g, 2.17 mmol), Cs_2CO_3 (2.121 g, 6.51 mmol) and acetone (60 mL) were heated at reflux under an inert atmosphere for 3 h. After cooling, acetone was evaporated in a rotavapor. The remaining solid was extracted with CH_2Cl_2 (3 × 50 mL) and filtered. The solvent was removed in a rotavapor and the white solid was washed with ethanol (2 × 50 mL) and hexanes (50 mL) and dried in vacuo; yield 0.651 g (67.3%). $[\alpha]_D^{25}$ = –224.1°mL dm^{-1} g^{-1} (c = 10 mg mL^{-1}, $CHCl_3$). IR (KBr): $\tilde{\nu}$ = 3067.5 (w), 1623.8 (w), 1591.4 (w), 1507.0 (m), 1475.7 (w), 1465.9 (w), 1437.2 (w), 1275.2 (s), 1267.9 (s), 1247.7 (m), 1199.8 (vs), 1182.3 (vs), 1154.9 (vs), 1096.3 (m), 1070.5 (s), 1030.2 (w), 978.6 (vs), 948.7 (s), 928.9 (vs), 881.5 (s), 864.5 (s), 835.1 (s), 815.4 (s), 782.1 (m), 750.9 (s), 713.0 (w), 695.5 (m), 655.7 (w) cm^{-1}. $^{31}P\{^1H\}$ NMR ($CDCl_3$): δ = 26.6 (octet) ppm.

X-ray Diffraction Analysis: X-ray crystal structures were collected with an Oxford Diffraction Gemini CCD diffractometer for **I** and with a Nonius Kappa CCD diffractometer for **II**. Both compounds were crystallized as described above to give block-shaped colourless crystals of **I** and white plate crystals of **II**.

The unit cell of **I** has a = 26.0158(9), b = 7.2275(2) and c = 18.8203(5) Å and shows a monoclinic symmetry C_2 with β = 96.336(3)°. R = 5.67454%. The absolute configuration of the molecule was confirmed by the Flack parameter = 0.08 (11). An unusual thermal displacement parameter (U_{eq}) ratio for the C atoms is a result of a comparison between carbon atoms with a very different mobility. This is confirmed by the above average U_{eq} values for some of them. The Hirshfeld rigid-bond test difference alert[23] for both the C28–C32 and C40–C41 bonds is due to some disorder still present in the structure after modelling. The same alert raised for the test performed on C35–C41 is due then to the same reason and, as this second test is associated with the standard uncertainty, it could be the result of over refinement. The search for possible solvent accessible voids was performed by using the VOID algorithm,[24] setting a grid of 0.20 Å and a probe radius of 1.20 Å for both **I** and **II**.

Compound **II** crystallized as white plate crystals, min., mid. and max. of 0.10, 0.30, and 0.60 mm, respectively. The unit cell has a = 32.9552(5), b = 5.5977(1) and c = 28.2450(7) Å, and shows a monoclinic symmetry C_2 with β = 120.9078(8)°, R = 8.21543%. The absolute configuration of the molecule was confirmed by the Flack parameter = 0.04(8). The different mobility of carbon atoms also results in an unusual carbon-atom U_{eq} ratio for compound **II**. The hydrogen atoms were all located in a difference map, but those attached to carbon atoms were repositioned geometrically. The hydrogen atoms were initially refined with soft restraints on the bond lengths and angles to regularize their geometry (C–H in the range 0.93–0.98 Å, N–H in the range 0.86–0.89 Å) and U_{iso}(H) (in the range 1.2–1.5 times U_{eq} of the parent atom), after which the positions were refined with riding constraints. The data collections were performed at 150 K and the strategy used aimed to achieve a complete data set for 2θ = 50°. Some higher-angle data were collected in the process and these have been included in the refinement.

The following software were used for the treatment and collection of data of **I**. CrysAlis[25a] to correct all systematic errors that lead to disparities in the intensities of symmetry-equivalent data (these may include absorption by the mount, crystal decay, changes in the volume of the crystal illuminated), the same software was used for the data collection carried out at 150 K and for cell refinement and data reduction, SIR92[25b] for structure solving, CRYSTALS[25c] for structure refinement and Mercury[25d] for molecular graphics. The following software packages were used for the treatment and collection of data of **II** performed at 150 K: Collect,[25e] Denzo/Scalepack[25f] for cell refinement and data reduction carried out at 150 K, SIR92[25b] for structure solving, CRYSTALS[25c] for structure refinement and Mercury[25d] for molecular graphics.

CCDC-756831 (for **II**) and -756832 (for **I**) contain the supplementary crystallographic data for this paper. These data can be obtained free of charge from The Cambridge Crystallographic Data Centre via http://www.ccdc.cam.ac.uk/data_request/cif.

MM Calculations: The Cerius2 package developed by BIOSYMJMSI was used to perform all the MM calculations through the OFF (Open Force-Field) routine in which the parameter set of the previously developed force field[16e,16j] was implemented. Periodic boundary conditions (PBC) were imposed for in-bulk calculations removing any symmetry constraint (P1). For non-bonding interactions (NB), a constant dielectric of ε = 1 and atomic charges obtained by the charge equilibration method, implemented in the Cerius2 package, were used. Moreover, a NB 1–4 scale factor of 0.5 and a SPLINE cut-off scheme (SPLINE-ON: 20 Å, SPLINEOFF: 30 Å) were used. All the energy optimizations were carried out by the conjugate gradient method, satisfying a gradient of $<$0.1 kJ Å mol^{-1}.

NMR Measurements: The room-temperature ^1H (499.88 MHz) and gCOSY NMR experiments were carried out at 300 K with a Varian Unity Inova 500 spectrometer equipped with a pulse-field gradient module (z axis) and a tunable 5-mm Varian Inverse detection probe (ID-PFG). Acquisition parameters for the ^1H NMR spectra were as follows: pulse width 7.3 μs, acquisition time 2.7 s, relaxation delay 2 s, spectral width 6 kHz, 32 K data points. The variable-temperature ^1H NMR spectra were acquired using a tunable 5-mm Varian Inverse detection probe (pulse width 7.3 μs). Samples were dissolved in $CDCl_3$ and the chemical shifts were referenced to external TMS.

Supporting Information (see also the footnote on the first page of this article): Detailed comment of the T-shaped interactions, all the numerical details of the ring puckering analysis and of the solvent accessible voids, together with g-COSY NMR spectra.

Acknowledgments

We are grateful to the Ministerio de Ciencia e Innovación de España for financial support (Project CTQ2007-61188).

[1] a) H. R. Allcock, *Chemistry and Applications of Polyphosphazenes*, Wiley, New York, **2003**; b) R. De Jaeger, M. Gleria, *Phosphazenes: A Worldwide Insight*, Nova Science Publishers, New York, **2004**.
[2] H. R. Allcock, *Acc. Chem. Res.* **1979**, *12*, 351–358.
[3] a) A. B. Chaplin, J. A. Harrison, P. J. Dyson, *Inorg. Chem.* **2005**, *44*, 8407–8417; b) M. Calichman, A. Derecskei-Kovacs, C. W. Allen, *Inorg. Chem.* **2007**, *46*, 2011–2016; c) L. Kapicka, P. Kubacek, P. Holub, *THEOCHEM* **2007**, *820*, 148–158.

[4] M. F. Bobrov, G. V. Popova, V. G. Tsirelson, *Russ. J. Phys. Chem.* **2006**, *80*, 584–590.
[5] H. R. Allcock, *Chem. Rev.* **1972**, 315–356.
[6] V. Chandrasekhar, B. Murugesapandian, *Acc. Chem. Res.* **2009**, *42*, 1047–1062.
[7] See ref.[1b], chapter 8, p. 171.
[8] E. W. Ainscough, A. M. Brodie, A. B. Chaplin, A. Derwahl, J. A. Harrison, C. A. Otter, *Inorg. Chem.* **2007**, *46*, 2575–2583.
[9] a) H. R. Allcock, A. P. Primrose, N. J. Sunderland, A. L. Rheingold, M. Parvez, I. A. Guzei, *Chem. Mater.* **1999**, *11*, 1243–1252; b) H. R. Allcock, E. N. Silverberg, G. K. Dudley, S. R. Pucher, *Macromolecules* **1994**, *27*, 7550–7555; c) H. R. Allcock, R. W. Allen, E. C. Bissell, L. A. Smeltz, M. Teeter, *J. Am. Chem. Soc.* **1976**, *98*, 5120–5125; d) P. Sozzani, A. Comotti, R. Simonutti, T. Meersmann, J. W. Logan, A. Pines, *Angew. Chem. Int. Ed.* **2000**, *39*, 2695–2698; e) H. R. Allcock, N. J. Sunderland, A. P. Primrose, A. L. Rheingold, I. A. Guzei, M. Parvez, *Chem. Mater.* **1999**, *11*, 2478–2485; f) A. Comotti, M. C. Gallazzi, R. Simonutti, P. Sozzani, *Chem. Mater.* **1998**, *10*, 3589–3596; g) H. R. Allcock, A. P. Primrose, E. N. Silverberg, K. B. Visscher, A. L. Rheingold, I. A. Guzei, M. Parvez, *Chem. Mater.* **2000**, *12*, 2530–2536.
[10] H. R. Allcock, E. N. Silverberg, G. K. Dudley, S. R. Pucher, *Macromolecules* **1994**, *27*, 7550–7555.
[11] G. Gahungu, B. Zhang, J. Zhang, *J. Phys. Chem. B* **2007**, *111*, 5031–5033.
[12] G. Gahungu, B. Zhang, J. Zhang, *J. Phys. Chem. C* **2007**, *111*, 4838–4845.
[13] G. A. Carriedo, F. J. García Alonso, J. L. García Alvarez, G. C. Pappalardo, P. Rossi, F. Punzo, *Eur. J. Inorg. Chem.* **2003**, 2413–2418.
[14] M. E. Amato, G. A. Carriedo, F. J. Garcia Alonso, J. L. Garcia Alvarez, G. M. Lombardo, G. C. Pappalardo, *J. Chem. Soc., Dalton Trans.* **2002**, 3047–3053.
[15] G. A. Carriedo, F. J. García Alonso, P. A. González, J. L. García Alvarez, *Macromolecules* **1998**, *31*, 3189–3196.
[16] a) G. C. Pappalardo, K. B. Lipkowitz, in: ref.[1b], chapter 11, pp. 237–256; b) R. Caminiti, M. Gleria, K. B. Lipkowitz, G. M. Lombardo, G. C. Pappalardo, *J. Am. Chem. Soc.* **1997**, *119*, 2196–2204; c) M. Gleria, K. B. Lipkowitz, G. M. Lombardo, G. C. Pappalardo, *Chem. Mater.* **1999**, *11*, 1492–1497; d) G. Bandoli, M. Gleria, G. M. Lombardo, G. C. Pappalardo, *J. Chem. Soc., Dalton Trans.* **1995**, *10*, 1749–1754; e) M. E. Amato, K. B. Lipkowitz, G. M. Lombardo, G. C. Papppalardo, *J. Mol. Struct.* **1995**, *372*, 69–84; f) G. Alberti, A. Grassi, G. M. Lombardo, G. C. Pappalardo, R. Vivani, *Inorg. Chem.* **1999**, *38*, 4249–4255; g) G. Alberti, G. M. Lombardo, G. C. Pappalardo, R. Vivani, *Chem. Mater.* **2002**, *14*, 295–303; h) G. A. Carriedo, F. J. Garcia-Alonso, J. L. García-Alvarez, G. M. Lombardo, G. C. Pappalardo, F. Punzo, *Chem. Eur. J.* **2004**, *10*, 3775–3782; i) G. M. Lombardo, G. C. Pappalardo, F. Punzo, F. Costantino, U. Costantino, M. Sisani, *Eur. J. Inorg. Chem.* **2005**, *24*, 5026–5034; j) G. M. Lombardo, G. C. Pappalardo, F. Costantino, U. Costantino, M. Sisani, *Chem. Mater.* **2008**, *20*, 5585–5592.
[17] M. E. Amato, R. Caminiti, G. A. Carriedo, F. J. García Alonso, J. L. García Alvarez, G. M. Lombardo, G. C. Pappalardo, *Chem. Eur. J.* **2001**, *7*, 1486–1494.
[18] G. A. Carriedo, F. J. García Alonso, P. A. González, *Macromol. Chem. Commun.* **1997**, *18*, 371–377.
[19] M. W. Hosseini, *Chem. Commun.* **2005**, 5825–5829.
[20] A. I. Kitajgorodskij, *Molecular Crystals and Molecules*, Academic Press, New York, **1973**.
[21] a) D. Cremer, J. A. Pople, *J. Am. Chem. Soc.* **1975**, *97*, 1354–1358; b) D. Cremer, *Acta Crystallogr., Sect. B* **1984**, *40*, 498–500; c) G. G. Evans, J. A. Boeyens, *Acta Crystallogr., Sect. B* **1989**, *45*, 581–590; d) J. C. A. Boeyens, *J. Cryst. Mol. Struct.* **1978**, *8*, 317–320; e) I. K. Boessenkool, J. C. A. Boeyens, *J. Cryst. Mol. Struct.* **1980**, *10*, 11–18.
[22] a) S. Grimme, *Angew. Chem. Int. Ed.* **2008**, *47*, 3430–3434; b) R. A. DiStasio Jr., G. von Helden, R. P. Steele, M. Head-Gordon, *Chem. Phys. Lett.* **2007**, *437*, 277–283; c) T. C. Dinadayalane, J. Leszczynski, *Struct. Chem.* **2009**, *20*, 11–20; d) T. Sato, T. Tsuneda, K. Hirao, *J. Chem. Phys.* **2005**, *123*, 104307; e) M. Rubes, O. Bludsky, P. Nachtigall, *ChemPhysChem* **2008**, *9*, 1702–1708.
[23] F. L. Hirshfeld, *Acta Crystallogr., Sect. A* **1976**, *32*, 239–244.
[24] P. van der Sluis, A. L. Spek, *Acta Crystallogr., Sect. A* **1990**, *46*, 194–201.
[25] a) *CrysAlis*, Oxford Diffraction Ltd., Abingdon, England, **2006**; b) A. Altomare, G. Cascarano, G. Giacovazzo, A. Guagliardi, M. C. Burla, G. Polidori, M. Camalli, *J. Appl. Crystallogr.* **1994**, *27*, 435; c) P. W. Betteridge, J. R. Carruthers, R. I. Cooper, K. Prout, D. J. Watkin, *J. Appl. Crystallogr.* **2003**, *36*, 1487; d) C. F. Macrae, P. R. Edgington, P. McCabe, E. Pidcock, G. P. Shields, R. Taylor, M. Towler, J. van de Streek, *J. Appl. Crystallogr.* **2006**, *39*, 453–457; e) COLLECT, Nonius BV, Delft, The Netherlands, **2001**; f) Z. Otwinowski, W. Minor, *Methods in Enzymology*, vol. 276, *Macromolecular Crystallography*, part A (Eds.: C. W. Carter Jr., R. M. Sweet), Academic Press, New York, **1997**, pp. 307–326.

Received: May 26, 2010
Published Online: August 4, 2010

